RSC Advances

ROYAL SOCIETY OF CHEMISTRY

www.rsc.org/advances

Fabrication of Polymer/Aligned Shish-Kebab Composite: Microstructure and Mechanical Properties

Haili Zheng, Yabo Quan, Guoqiang Zheng,* Kun Dai, Chuntai Liu,* and Changyu Shen

College of Materials Science and Engineering, The Key Laboratory of Material Processing and Mold of Ministry of Education, Zhengzhou University, Zhengzhou, 450002, P.R. China

Corresponding Authors: Guoqiang Zheng (gqzheng@zzu.edu.cn), Chuntai Liu (ctliu@zzu.edu.cn).

Tel.: +86 371 63887600

Abstract

Shear-induced ultrahigh molecular weight polyethylene (UHMWPE) shish-kebab mat (USKM), in which shish-kebabs are well aligned, has been achieved from dilute UHMWPE solution. Such USKM is incorporated into linear low density polyethylene (LLDPE) as reinforcement filler. Isothermal crystallization shows that the USKM acts as an effective nucleating agent for LLDPE crystallization, leading to enhanced crystallinity, long period and lamellar thickness of USKM/LLDPE composite. Instead of shish-kebabs, only aligned fibrils are observed in the composite. Such fibrils consist of shish structure wrapped with LLDPE chains and good bonding at the

interface between the fibril and matrix is achieved. Consequently, the interfacial adhesion is expected to be improved and favorable stress transfer is realized. Together with good bonding, superior strength of shish and the above enhanced crystalline parameters contribute to a significant increment in tensile strength and modulus of the composite, as compared to pure LLDPE.

Keywords: Shish-kebab mat, Linear low density polyethylene, Compression moulding, Interfacial interaction, Mechanical properties

1. Introduction

Shish-kebab structure has attracted tremendous attentions since it was firstly observed in sheared dilute polyethylene solution.[1-3] As well documented, this structure typically consists of an extended-chain central fibrillar core forming shish and disk-like folded chain crystals forming kebabs, which are always oriented perpendicularly to the shish.[4-8] Shish-kebabs are well known to be induced by flow, such as in the sheared dilute polymer solutions,[2,3] sheared or stretched polymer melts.[9-11] As a highly oriented structure, shish-kebab is endowed with superior strength and modulus along its longitudinal axe,[7,8] providing the potential to fabricate self-reinforced polymer products.[12-15] The content of shish-kebabs has become a decisive factor for enhancement of polymer products.[9,16,17] However, products fabricated by common processing methods cannot get reinforced as expected. Take injection-moulded parts as an example: very small amount of shish-kebabs can be in-situ developed in the final injection-moulded parts, and moreover they are only located in an extremely thin layer close to the surface due to the intense shear and fast

solidification therein.[18,19] Whereas, numerous spherulites instead of shish-kebabs are always developed in a very broad inner layer due to weak shear and sufficient relaxation of chains caused by slow cooling of melts therein.[20]

To date, studies on semi-crystalline polymers (*e.g.*, polyethylene and polypropylene) based composites have indicated that reinforced fillers are roughly classified into two categories: inorganic and organic ones. Due to the extraordinary mechanical properties, a wide range of inorganic fillers including clay,[21-24] calcium carbonate,[25,26] carbon nanotube,[27,28] *etc.*, have been utilized to prepare reinforced composites. As for the organic fillers, various types have attracted more and more attentions because of their good compatibility with polymer matrix, such as polymer fiber[29,30] and electrospun polymer nanofiber.[31,32] In view of some intrinsic features of shish-kababs, *e.g.*, superior strength and modulus along the longitudinal axes and the huge potential to fabricate self-reinforced polymer products, we are wondering whether shish-kebabs could be used as reinforcement filler and directly incorporated into heterogeneous matrix to realize the reinforcement of polymer matrix. If so, this method can also overcome the aforementioned problem that products fabricated by common processing methods cannot get reinforced as expected due to the limited amount of shish-kebabs. Nevertheless, study concerning this has been scarcely reported. The reasons may be as follows: (1) with respect to the shish-kebabs obtained from the sheared dilute polymer solutions, common blending with heterogeneous matrix may take risk of destroying the as-prepared oriented structure of shish-kebabs; (2) the content of shish-kebabs obtained from sheared or stretched polymer melts is

extremely low, and moreover it is impossible for them to be detached completely from the total products.

In this study, our interest is to explore the feasibility of direct introduction of the shish-kebabs into heterogeneous polymer matrix as an ideal reinforced element. Ultrahigh molecular weight polyethylene (UHMWPE) shish-kebab mat (USKM) was firstly prepared through shear-induced crystallization of UHMWPE solution and then incorporated into linear low density polyethylene (LLDPE) matrix. Subsequently, compression moulding was utilized to fabricate USKM/LLDPE composite. Results indicate that even a small amount of USKM can notably enhance the LLDPE matrix. This work opens a new gateway for direct incorporating the shish-kebabs into polymer matrix with the purpose of preparing high-performance polymer products.

2. Experimental section

2.1 Materials

UHMWPE powder was provided by Second Auxiliary Factory, Beijing, China, with a number-average molecular weight (M_n) in the range of 2.0-3.0 × 10^6 g/mol. The nominal melting point of it is 142 ^oC (obtained by differential scanning calorimetre (DSC) method, sample with 5-8 mg was heated to 180 ^oC from room temperature at a heating rate of 10 ^oC/min). Commercially available LLDPE (Trade marked as 7042) with melt flow index (MFI) of 2.0 g/10 min (190 ^oC, 2.16 kg), weight-average molecular weight (M_w) of 1.4 × 10^5 g/mol, was supplied by Maoming Petrochemical Corp., China. Its density is 0.92 g/cm^3. Xylene (analytical reagent, 99%) was bought from Tianjin Chemical Reagents Plant.

2.2 Fabrication of shear-induced USKM

Shear-induced USKM was fabricated through shear-induced crystallization of UHMWPE solution. UHMWPE powder was firstly dissolved completely in xylene at 140 ^{o}C to obtain the UHMWPE solution with a concentration of 0.01 wt % and then rapidly transferred into a bath pot whose temperature was 105 ^{o}C. Shear-induced crystallization was carried out at this temperature using a mechanical stir bar at a speed of 500 rpm, which is shown in Figure 1a. Ferrum frames were fixed on the stir bar so that the frames could rotate synchronously with the stir bar. Thus, the UHMWPE solution was subject to shear arising from the rotating ferrum frames on which USKM can be collected. After shear-induced crystallization for 30 min, the collected shish-kebab mat was taken out from the solution and washed with xylene to remove free polymers. Before characterizations, the mat was dried at room temperature for 24 hours (see Figure 1b).

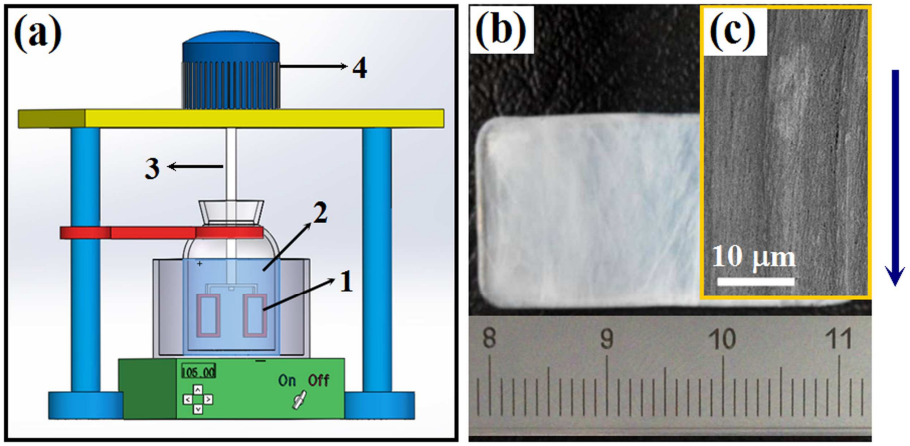

Figure 1. (a) Schematic of the shear-induced crystallization setup used in this study; (b) digital photo of the shear-induced USKM; (c) SEM image of the shear-induced USKM with low magnification. The numbers in (a) represents: 1-ferrum frame; 2-UHMWPE/xylene solution; 3-stir bar; 4-motor. The blue arrow in (b) refers to the shear direction.

2.3 Composite preparation

In view of interfacial adhesion, polyethylene (PE), such as, high density

polyethylene (HDPE), LLDPE, *etc.*, must be the ideal candidates acting as matrix because they have the same monomer as that of UHMWPE.[16,33] Moreover, the prerequisite for realizing the reinforcement of composite is that USKM must be intact as much as possible when the matrix is in the molten state during compression moulding. To this end, melting behaviors of the candidates (*e.g.*, HDPE, LLDPE) should be taken into account. As shown in Figure 2, the melting zone of the shear-induced USKM generally ranges from 120 °C to 150 °C. That is to say, the end melting point of the candidates must be near or below 120 °C (*viz.*, onset melting point of the USKM) in order to preserve the as-prepared USKM. However, melting of the as-received HDPE ends at about 137 °C, at which the USKM must be partially melted (see Figure 2). As for LLDPE, the end melting point is about 125 °C, very close to the onset melting point of the USKM (120 °C). Therefore, LLDPE is the ideal candidate because the USKM would be maintained almost intact when LLDPE is completely melted at about 125 °C.

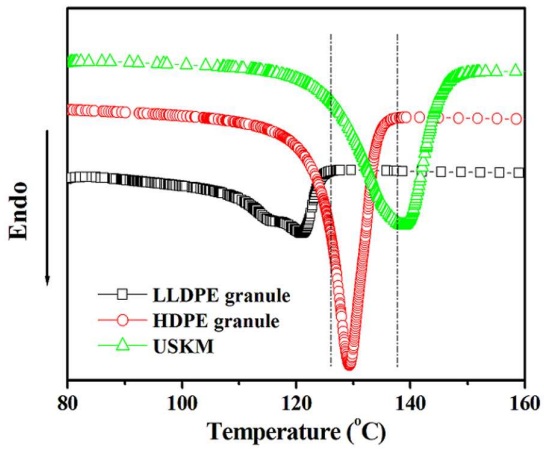

Figure 2. DSC melting curves of the as-received LLDPE, HDPE granules and shear-induced USKM (samples with 5-8 mg were respectively heated to 180 °C from room temperature at a heating rate of 10 °C/min).

The USKM/LLDPE composite was prepared according to the following procedures.

After shear-induced crystallization and drying process, USKM supported by ferrum frames was obtained. However, USKM was not stripped off from ferrum frames in order to avoid the shrinkage of USKM. Firstly, the shear-induced USKM supported by ferrum frame was preheated to 100 ^{o}C. Then, the LLDPE/xylene solution with a concentration of 10 wt % was casted on only a piece of USKM supported by ferrum frame. Thus, the USKM cannot float on the surface of the LLDPE solution due to the support of the ferrum frame. After the solvent was completely evaporated, the USKM was stripped off from the ferrum frame. The USKM/LLDPE composite was finally obtained by a vacuum-assisted compression moulding machine (FM-11, Beijing Future Materials Science-Technology Co., Ltd.). The benefit of such vacuum-assisted compression moulding machine is twofold: on one hand, oxidative degradation will not occur under vacuum condition; on the other hand, compared with the common compression moulding machine, such machine can eliminate the bubbles in the compressed samples as much as possible. The detailed scenario of the compression moulding process was interpreted as follows: the casted USKM/LLDPE composite film was preheated at 130 ^{o}C for 10 min and pressed at a pressure of 0.3 MPa for 5 min, followed by isothermal crystallization at 115 ^{o}C for 1 hour. After that, it was cooled to room temperature and the USKM/LLDPE composite was finally obtained. The concentration of USKM in the USKM/LLDPE composite was 0.8 wt % and its calculated method can be found in Supplementary Information. For comparison purpose, pure LLDPE film in the absence of USKM was also prepared under the same conditions described above.

2.4 Characterization

Macroscopic USKM was first observed by a digital camera (Sony WX9).

To better characterize the surface morphology of the shear-induced USKM,

scanning electron microscope (SEM, JEOL JSM 7500F) was employed under an acceleration voltage of 5 kV. Moreover, SEM measurement was also adopted for identifying interfacial interaction between the UHMWPE shish-kebabs and matrix. Before SEM observation, the compression moulded USKM/LLDPE composite as well as pure LLDPE was etched according to our previous work.[34] The samples were sputtered with gold before observation.

Atomic force microscope (AFM, SPM-9500J3, Japan) was also empolyed to observe the surface morphology of the shear-induced USKM. It was conducted at ambient conditions (25 ^{o}C) using tapping mode probes with constant amplitude. AFM image was recorded at the resonance frequency of the cantilever with a scan rate of 1 Hz. Moreover, the AFM image was taken at 256 × 256 pixels.

In order to clarify the nucleating effect of USKM towards LLDPE, isothermal crystallization was conducted using differential scanning calorimetry (TA DSC-2920) under a pure nitrogen atmosphere. Both the USKM/LLDPE composite and pure LLDPE with 5-8 mg were respectively heated to 130 ^{o}C at a heating rate of 10 ^{o}C/min and held for 2 min to erase the possible thermo-mechanical history. And then, the samples were quickly cooled down to 115 ^{o}C at a cooling rate of 30 ^{o}C/min for isothermal crystallization. The melting behaviors of the USKM/LLDPE composite and pure LLDPE were also investigated. The detailed scenario of DSC melting measurement was set as follows: samples with 5-8 mg were heated to 180 ^{o}C at a heating rate of 10 ^{o}C/min.

Two-dimensional wide angle X-ray diffraction (2D-WAXD) and two-dimensional

small angle X-ray scattering (2D-SAXS) experiments were both conducted at the beamline BL16B1 of the Shanghai Synchrotron Radiation Facility (SSRF). X-ray beam with a wavelength of 0.124 nm was used. To collect 2D-WAXD and 2D-SAXS patterns, a Mar165CCD detector (2048 × 2048 pixels with pixel size 80 μm) was employed. The samples were placed with the orientation (shear direction) perpendicular to the incident X-ray beam. The data acquisition time was 60 s per frame. For all the 2D-WAXD and 2D-SAXS profiles, the amorphous background was extracted. It should be noted that, for X-ray measurements, to get the maximum diffraction/scattering intensity, several samples were stacked orderly (*viz.*, all the stacked samples were parallel along the shear direction) to obtain the total thickness of about 1 mm.

Tensile test was carried out on a Linkam TST350 tensile stage with a 200 N load cell. Rectangular specimens with width of 5 mm and length of 10 mm were cut from centre of the compression moulded samples along the shear direction (see Figure S1 in Supplementary Information). The tensile direction was along the orientation direction of the shish-kebabs. The pulling speed was 100 μm/s and the measured temperature was around room temperature (25 ^{o}C). The reported values were calculated as average over at least five specimens.

3. Results and discussion

3.1 Morphology of shear-induced USKM

Figure 1b shows the macroscopic morphology of USKM obtained via shear-induced crystallization. SEM image with low magnification in Figure 1c

demonstrates that the USKM is composed of numerous fibrils oriented along the shear direction. Furthermore, detailed morphology observed by SEM with high magnification is shown in Figure 3. It can be evidently seen that these fibrils are aligned orderly along the shear direction despite locally disordered arrangement. The amplified image reveals that all these fibrils consist of a single fibrillar core and many crystalline lamellae decorated perpendicularly to the fibrillar core (see Figure 3b). Such characteristics confirm that the fibrils are typical shish-kebabs.[4,5] Nevertheless, there exists obvious breakage in shish-kebabs shown by white arrows in Figure 3b, which should be resulted from high voltage exerted on these feeble shish-kebabs. Furthermore, though the shish-kebabs are densely arranged shown in Figure 3, explicit voids are present between them, leading to potential possibility for LLDPE/xylene solution penetration. In addition, the formation of the aforementioned shish-kebabs in the dilute UHMWPE solution under shear flow can be best explained using the concept of coil-stretch transition proposed by de Gennes[35]: the UHMWPE chains are generally in an equilibrium coiled state in the dilute solution. Once shear flow is exerted, the long coiled chains could be stretched along the shear direction and then crystallize into shish, on which, the short coiled chains are subsequently adsorbed and form kebabs.[36]

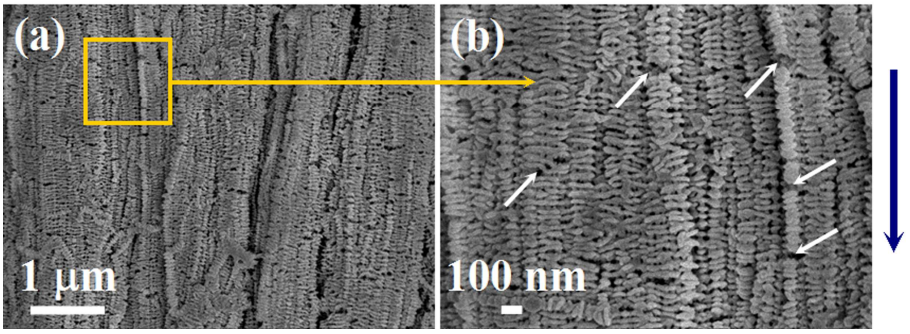

Figure 3. SEM images of the shear-induced USKM. The blue arrow refers to the shear direction.

AFM was also employed to observe the detailed surface morphology of the shear-induced USKM (1.25 × 1.25 μm), as displayed in Figure 4. Individual lamellae can be easily identified. These UHMWPE lamellae are highly aligned along the shear direction. Combined with the detailed morphology observed by SEM shown in Figure 3, it can be safely concluded that the aligned lamellae shown in Figure 4 are actually shish-kebab structure. However, the kebabs are so compact that shish is invisible. On the whole, the AFM image is another evidence that well aligned shish-kebabs have been prepared in this study.

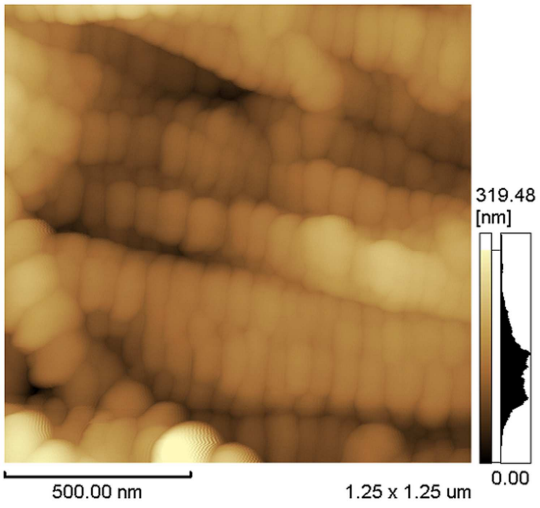

Figure 4. AFM image of the shear-induced USKM. The shear direction is horizontal.

3.2 Effect of USKM on isothermal crystallization behavior of LLDPE

In order to detect the nucleating effect of the USKM towards LLDPE, isothermal

crystallization experiments at 115 °C for both USKM/LLDPE composite and pure LLDPE were carried out. The isothermal crystallization exotherms of the two samples are shown in Figure 5a. The normalized relative crystallinity (X_t) is obtained from the ratio of the exothermic peak area at a given crystallization time (t) to the total area of this exothermic peak, *i.e.*,

$$X_t = \int_0^t (dH/dt)dt \Big/ \int_0^\infty (dH/dt)dt \quad (1)$$

where dH/dt is the heat flow rate.

The normalized relative crystallinity versus time for the two samples is shown in Figure 5b. It is evident that the isotherms exhibit a sigmoid dependence with time. The USKM/LLDPE composite yields shorter induction time (0.3 min) and completion time (3.9 min), while pure LLDPE has longer induction time (1.0 min) and completion time (7.1 min). That is to say, crystallization process of the composite seems to proceed steadily faster than the pure sample. Furthermore, half crystallization time ($t_{1/2}$) is also obtained and presented in Figure 5b. Obviously, $t_{1/2}$ of the USKM/LLDPE composite and pure LLDPE is 1.4 min and 2.5 min, respectively. In other words, the crystallization rate of the composite increases about 1.8 times of that for the pure LLDPE, suggesting that the USKM could act as an effective nucleating agent for LLDPE crystallization.[37,38]

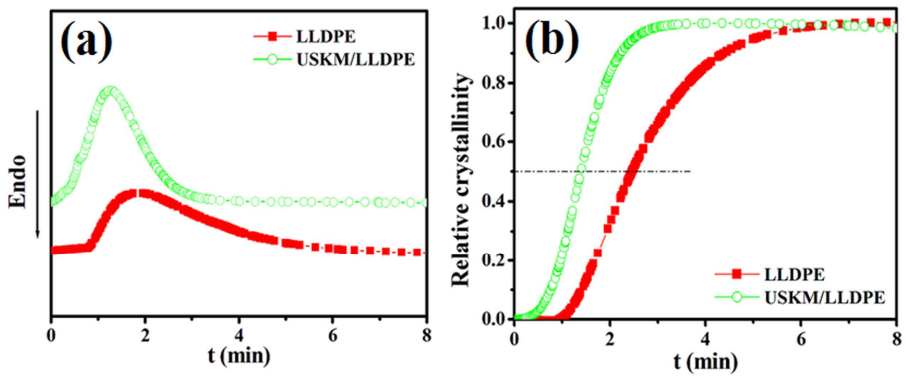

Figure 5. (a) DSC curves of isothermal crystallization for USKM/LLDPE composite and pure LLDPE; (b) normalized relative crystallinity (X_t) as a function of crystallization time.

3.3 Microstructure of USKM/LLDPE composite

2D-WAXD and 2D-SAXS measurements were carried out to investigate the crystalline and lamellar structure of pure LLDPE and USKM/LLDPE composite, and the results are shown in Figure 6. According to 2D-WAXD patterns, only isotropic diffraction circles designated to the $(110)_o$ plane and $(200)_o$ plane of orthorhombic lamellae can be observed for pure LLDPE, indicating a random arrangement of molecular chains.[39] With respect to the USKM/LLDPE composite, apart from the typical $(110)_o$ plane and $(200)_o$ plane, additional wide diffraction arcs designated to the $(200)_m$ plane of monoclinic cell are also observed. Combined with the aforementioned results of pure LLDPE, it is obvious that this $(200)_m$ plane is ascribed to the incorporation of shear-induced USKM.[40] Moreover, Figure 7a shows the azimuthal distribution integrated from the $(200)_m$ plane of USKM/LLDPE composite. Clearly, two wide peaks, exhibiting a broad azimuthal width, are respectively located at 90° and 270° on the azimuthal curve. It seems that USKM incorporated into LLDPE matrix shows low orientation level. However, as shown in Figure 3, 4, shish-kebabs in the as-prepared mat are well aligned. Therefore, one can conclude that the original orientation structure is maintained to some extent despite inevitable relaxation of oriented molecules or disorder of shish-kababs occurred during the compression moulding process. Furthermore, isotropic diffraction circle referring to the $(110)_o$ crystal plane of the USKM/LLDPE composite shown in Figure $6a_2$ demonstrates that oriented structure in LLDPE matrix is not formed during the compression process after the incorporation of the shear-induced USKM.

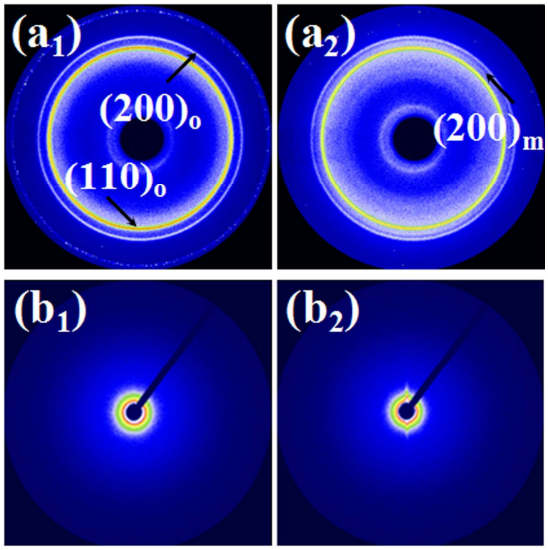

Figure 6. 2D-WAXD (a_1, a_2) and 2D-SAXS (b_1, b_2) patterns of samples: pure LLDPE (a_1, b_1), USKA/LLDPE composite (a_2, b_2). The shear direction of USKM is horizontal.

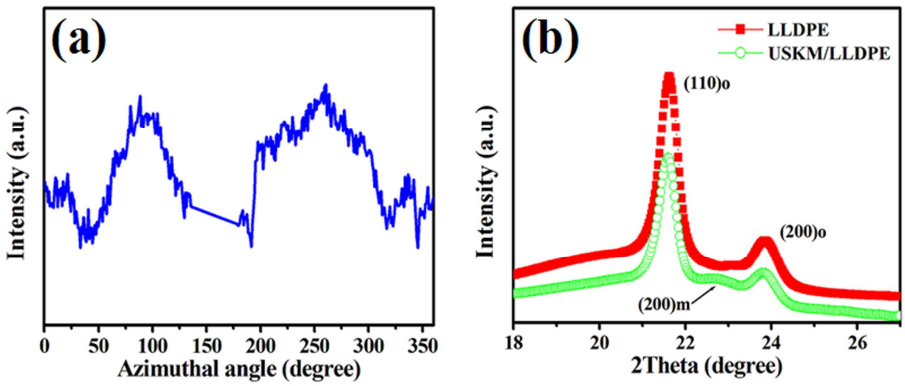

Figure 7. (a) Azimuthal distribution integrated from $(200)_m$ crystal plane of USKM/LLDPE composite; (b) 1D-WAXD curves of pure LLDPE and USKM/LLDPE composite.

Similar to the 2D-WAXD pattern for the pure LLDPE, 2D-SAXS pattern of pure LLDPE is also isotropic, manifesting that spherulites prevail herein. Whereas, with respect to the USKM/LLDPE composite, the 2D-SAXS pattern exhibits a streak along the meridian with no evidence of equatorial maxima. Considering that LLDPE chains are not oriented obviously (see the 2D-WAXD results), it can be deduced that the meridianal streak is originated from the shish structure in USKM. This is another

evidence that the incorporated USKM is not completely destroyed during the compression moulding process and the original oriented structure shown in Figure 3 and Figure 4 can be preserved even subjected to high temperature during compression moulding process.

To quantify the crystalline content, one-dimensional (1D) WAXD profiles were derived from Figure 6 through circularly integrating intensity of 2D-WAXD patterns (shown in Figure 7b). Then a Gaussian fitting of multipeaks was utilized to obtain the areas of crystalline and amorphous peaks. The overall crystallinity (X_c) was calculated according to the following equation[41]

$$X_c = \frac{\sum A_{cryst}}{\sum A_{cryst} + \sum A_{amorp}} \times 100\% \quad (2)$$

where A_{cryst} and A_{amorp} are the fitted areas of crystalline and amorphous regions, respectively. The overall crystallinity is listed in Table 1. Obviously, compared with pure LLDPE, an increase in X_c for USKM/LLDPE composite is achieved, which is ascribed to the heterogeneous nucleating effect of USKM towards LLDPE. The heterogeneous nucleation could prompt the normally noncrystallizing LLDPE chains to crystallize, leading to an increment in final crystallinity.[42]

Table 1. The crystalline parameters obtained from the 2D-WAXD and 2D-SAXS results.

Samples	X_c (%)	L_c (nm)	L (nm)
LLDPE	36.44	5.68	12.78
USKM/LLDPE	39.13	5.80	13.02

From the 2D-SAXS intensity, one-dimensional correlation function (Strobl method) $K(z)$ is calculated by cosine Fourier transformation[43]

$$K(z) = \frac{1}{r_e^2 (2\pi)^3} \int_0^\infty \cos(qz) 4\pi q^2 \sum(q) dq \quad (3)$$

where q is the scattering vector $q = 4\pi \sin\theta_B / \lambda$, θ_B denotes the Bragg angle, $\sum(q)$ is the differential cross section per unit volume and r_e is the classical electron radius. Figure 8a presents an example of the one-dimensional electron density correlation function. As indicated by the black arrows, this curve can give various structural parameters, *e.g.*, long period (L) and lamellar thickness (L_c), according to the methodology proposed by Strobl et al.[43,44] Figure 8b shows the one-dimensional correlation function for pure LLDPE and USKM/LLDPE composite. For the purpose of quantitative analysis, the value of L, L_c obtained from the correlation functions is listed in Table 1. Obviously, USKM/LLDPE composite exhibits larger L and L_c. Moreover, the aforementioned results show that higher crystallinity of the USKM/LLDPE composite is also achieved. Consequently, it is reasonable to claim that the increment of these crystalline parameters (L, L_c, X_c) is attributed to the incorporation of USKM. As an effective nucleating agent for LLDPE (see the DSC results shown in Figure 5), USKM can provide heterogeneous nucleation sites for LLDPE matrix and enhance the crystallization kinetics, consequently leading to higher crystallinity and thicker lamellae.[45]

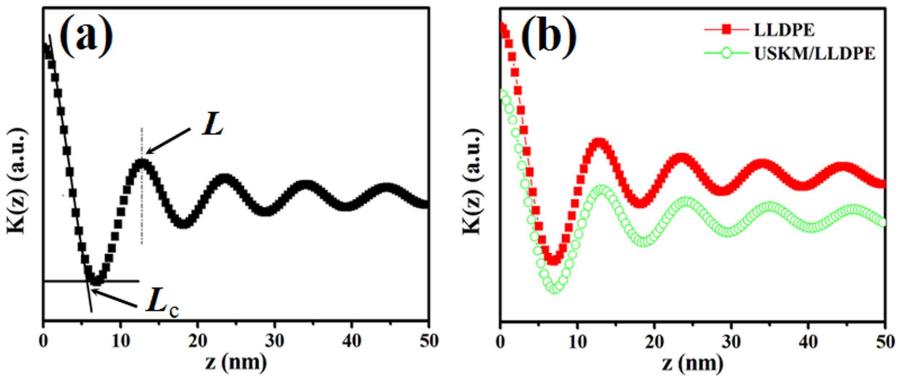

Figure 8. (a) Calculation method of long period (L), lamellar thickness (L_c) obtained from the one-dimensional correlation function $K(z)$; (b) curves of the one-dimensional electron density correlation function of the pure LLDPE and USKM/LLDPE composite.

3.4 Interfacial feature between incorporated shish-kebabs and matrix

Interfacial feature between the shear-induced shish-kebabs and matrix in the composite was observed by SEM. As shown in Figure 9a, some fibrils indicated by blue arrows can be clearly observed in the composite. Owing to incomplete etching, not all fibrils can be substantially exposed. However, more fibrils can be clearly found in Figure S2 with lower magnification shown in Supplementary Information. Considering the fact that oriented structure of LLDPE matrix is not developed during the compression moulding process after the incorporation of the shear-induced USKM, these fibrils must be shish originated from USKM in the absence of kebabs. However, the diameter of the fibrils indicated by blue arrows (see Figure 9b) seems to be much larger than the original shish structure shown in Figure 3 and Figure 4. In terms of the effective nucleating effect of USKM towards LLDPE, one can conclude that such shish structure is substantially wrapped with LLDPE molecules, forming the fibrils shown in Figure 9 during the compression moulding process. Once again, SEM

observation is another evidence that shish structure in the USKM acts as nucleating templates for LLDPE matrix crystallization.

Figure 9a also shows that these fibrils are generally parallel to each other, implying that the original oriented structure of shish-kebabs has been maintained to some extent. Of note, kebabs are not observed on these fibrils. This may be due to weaker stability of kebabs and relaxation of them during the compression moulding process.[28] In addition, the observed fibrils are not densely distributed as those shish-kebabs shown in Figure 3 and Figure 4, which might be ascribed to the two following reasons: on one hand, the fibrils are not exposed substantially due to incompletely etching as mentioned above; on the other hand, relaxation of shish-kebabs with small size occurs during the compression moulding process.

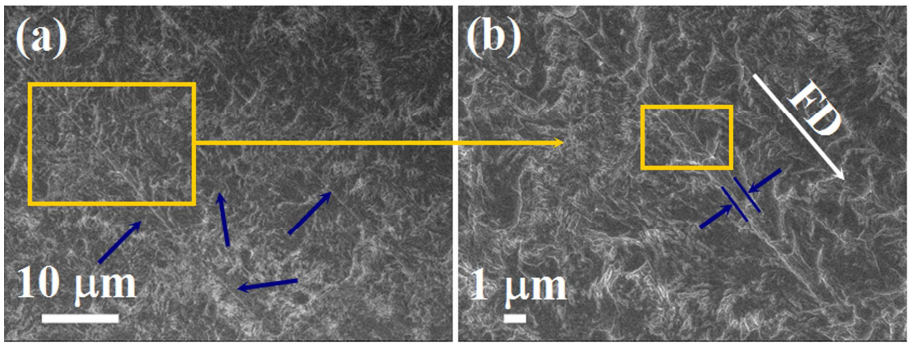

Figure 9. SEM images of etched surface of USKM/LLDPE composite. The white arrow refers to flow direction of USKM.

Moreover, good bonding between the fibrils and matrix is achieved because gap or groove cannot be observed at the interface (see Figure 9b). The nucleating role together with good bonding at the interface between the fibrils and matrix is expected to produce anchoring of LLDPE molecules to the fibrils and thus to improve the adhesion, generating better stress transfer and higher mechanical properties of the

USKM/LLDPE composite compared to pure LLDPE.[46]

3.5 Thermal behaviors

The DSC melting curves of pure LLDPE and USKM/LLDPE composite are exhibited in Figure 10a. As can be seen, there are two melting peaks for the pure LLDPE. One sharp peak (primary peak) locates at around 121.5 ^{o}C corresponding to the fusion of stable crystals with thicker lamellae, while the other shoulder peak appearing at 115 ^{o}C is attributed to the melting of small or imperfect crystals containing thinner lamellae. It is well known that incorporation of α-olefins in the polyethylene backbone allows LLDPE to have many short chain branches (SCBs). The short chain length and its distribution in the polymeric chains of the LLDPE are not uniform, resulting in crystals with a wide distribution of lamellar thickness.[47] As for the USKM/LLDPE composite, the primary peak seems to become sharper and shifts to a higher temperature (122.5 ^{o}C), as compared to that of the pure LLDPE. Furthermore, the shoulder peak at about 114.9 ^{o}C is almost absent. The reasons for this may be that the SCBs are prone to participating in the formation of thicker lamellae due to the effective heterogeneous nucleating effect of USKM towards LLDPE matrix. However, the melting peak of USKM at around 138.6 ^{o}C shown in Figure 2 can not be observed in the melting curve of the USKM/LLDPE composite (see Figure 10b). The reason leading to this can be understood that the content of USKM incorporated into LLDPE matrix is extremely low (only 0.8 wt%) and difficult to be detected by DSC technique.[48]

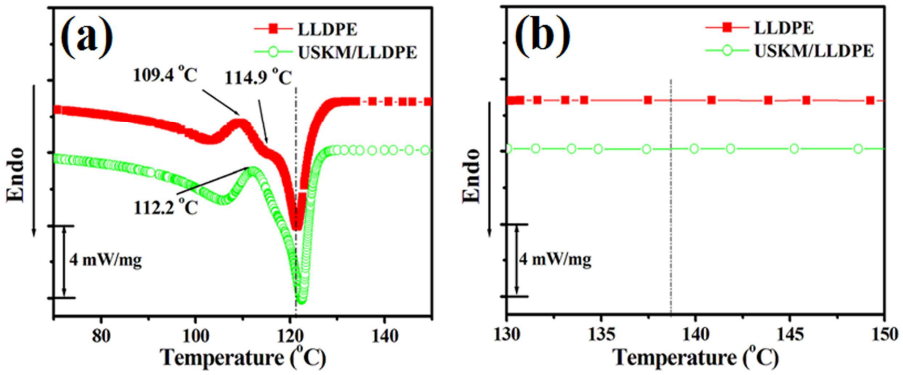

Figure 10. (a) DSC melting curves of pure LLDPE and USKM/LLDPE composite; (b) amplified image of the area in the dashed square of (a).

It is also worth mentioning that a crystallization peak for pure LLDPE emerges at 109.4 °C. As elucidated above, owing to the existence of SCBs and nonuniform short chain length as well as its nonuniform distribution in the LLDPE chains, lamellar structure with a wide distribution of thickness could be formed.[47] When melting experiment is conducted, the tiny and imperfect crystals will firstly melt, whereas the thicker or perfect ones are stable and remain intact. Then the molten chains of tiny and imperfect crystals will self-nucleate and recrystallize once the crystallization temperature of LLDPE (109.4 °C) has been reached. Thus, crystallization peak located at about 109.4 °C could be formed during the heating scan. However, such crystallization peak shifts to 112.2 °C for the USKM/LLDPE composite. This phenomenon could be ascribed to the heterogeneous nucleation of USKM towards LLDPE, leading to enhanced crystallization kinetics and higher crystallization temperature.[37,49] The crystallinity (X_c) of the two samples was calculated by the equation

$$X_c = \frac{\Delta H_i}{\varphi_i \Delta H_i^m} \times 100\% \quad (4)$$

where ΔH_i is the enthalpy of fusion and φ_i is the weight fraction of the matrix polymer (LLDPE). Herein, ΔH_i^m is the enthalpy of fusion for 100% crystallized PE, which is adopted as 293 J/g.[50] The calculated crystallinity of the pure LLDPE and USKM/LLDPE composite are 47.2%, 55.0%, respectively. That is to say, crystallinity of the USKM/LLDPE composite is higher than that of the pure LLDPE, which is well in line with the calculated results from 2D-WAXD.

3.6 Tensile test

The representative stress-strain curves of pure LLDPE and USKM/LLDPE composite are shown in Figure 11. In order to quantitatively estimate the variations of mechanical properties, the values of mechanical parameters, *e.g.*, yield strength (σ_y), ultimate tensile strength (σ), Young's modulus (E) and elongation at break (ε) are obtained from the stress-strain curves and summarized in Table 2. One can clearly see that LLDPE matrix has been steadily reinforced due to the incorporation of shear-induced USKM. For example, the Young's modulus, a manifestation of stiffness, rises from 80.6 MPa for pure LLDPE to 112.5 MPa for USKM/LLDPE composite. At the same time, compared with the pure LLDPE, the composite exhibits a dramatic improvement in yield strength, from 5.5 MPa to 10.5 MPa with an increment of 90.9%. The ultimate tensile strength is also elevated from 13.2 MPa for pure LLDPE to 16.1 MPa for USKM/LLDPE composite. The mechanisms of superior mechanical reinforcement will be discussed based on the aforementioned microstructural investigations.

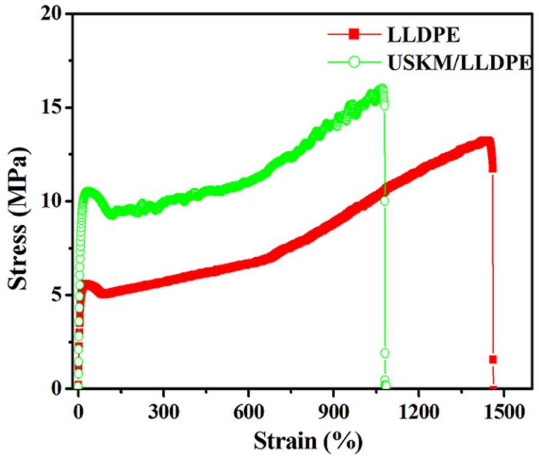

Figure 11. Representative stress-strain curves of pure LLDPE and USKM/LLDPE composite.

Table 2. Mechanical parameters obtained from stress-strain curves.

Samples	E (MPa)	σ_y (MPa)	σ (MPa)	ε (%)
LLDPE	80.6 ± 5.3	5.5 ± 0.7	13.2 ± 0.6	1468.0 ± 32
USKM/LLDPE	112.5 ± 4.6	10.5 ± 1.2	16.1 ± 0.8	1084.2 ± 45

It is well established that the macroscopic mechanical performance of the composite is determined by many microstructural factors, such as interfacial interaction, orientation level of incorporated shish-kebabs and matrix crystalline phase, crystalline characters (*e.g.*, L, L_c, X_c) and so on.[50] However, according to 2D-WAXD and 2D-SAXS results, no obvious orientation of matrix is detected. It is reasonable to deduce that the effect of orientation level in matrix on mechanical enhancement of the composite can be ruled out. Owing to the strong nucleating role of the shish structure towards LLDPE matrix, the interfacial adhesion and stress transfer between shish and LLDPE matrix must be enhanced (see Figure 9). Moreover, the aligned fibrils containing shish and its superior strength will play important role in the reinforcement of matrix. In addition, mechanical properties of semi-crystalline polymers generally depend on the content of the crystalline domains. Thus, the

enhanced X_c must be responsible for mechanical strengthening of the composite. Meanwhile, as well established in other studies,[51,52] the increased L and L_c also contribute to the enhanced tensile properties. Therefore, the increased X_c, L and L_c of the USKM/LLDPE composite as well as the alignment and reinforcement of shish synergistically contribute to the increases in mechanical properties of the USKM/LLDPE composite.

4. Conclusions

In this study, ultrahigh molecular weight polyethylene (UHMWPE) shish-kebab mat (USKM), in which shish-kebabs are well aligned with each other, has been achieved through shear-induced crystallization. Then the USKM is incorporated into heterogeneous matrix to prepare reinforced composite. Via isothermal crystallization experiments, it is concluded that the USKM is highly effective in nucleating LLDPE matrix, leading to increased crystallinity, long period and lamellar thickness for the composite. Because shish is wrapped with LLDPE molecules, better interfacial adhesion and stress transfer can be achieved. Together with the superior strength of shish structure, the aforementioned crystalline characters and better interfacial adhesion synergistically contribute to the mechanical reinforcement of the USKM/LLDPE composite. As a new method of utilizing shish-kebabs as filler to prepare reinforced products, we believe that the compression moulded USKM/LLDPE composite holds a promising application in preparing high-performance products. Further study will be carried out to realize the application of USKM in the preparation of high-performance composites.

Acknowledgements

We express our great thanks to the National Natural Science Foundation of China (51173171, 11172271), HASTIT of Henan Province and State Key Laboratory of Materials Processing and Die & Mould Technology for financial support.

References

1 A. Pennings and A Kiel, *Colloid. Polym. Sci.*, 1965, **205**, 160-162.
2 A. Peterlin, *Pure Appl. Chem.*, 1966, **12**, 563-586.
3 A. Peterlin, *Adv. Macromol. Chem.*, 1968, **1**, 225.
4 B. S. Hsiao, L. Yang, R. H. Somani, C. A. Avila-Orta and L. Zhu, *Phys. Rev. Lett.*, 2005, **94**, 117802.
5 W. Hu, D. Frenkel and V. B. Mathot, *Macromolecules*, 2002, **35**, 7172-7174.
6 L. Balzano, N. Kukalyekar, S. Rastogi, G. W. Peters and J. C. Chadwick, *Phys. Rev. Lett.*, 2008, **100**, 048302.
7 J. Odell, D. Grubb and A. Keller, *Polymer*, 1978, **19**, 617-626.
8 Z. Bashir, J. Odell and A. Keller, *J. Mater. Sci.*, 1984, **19**, 3713-3725.
9 H. R. Yang, J. Lei, L. Li, Q. Fu and Z. M. Li, *Macromolecules*, 2012, **45**, 6600-6610.
10 O. O. Mykhaylyk, P. Chambon, C. Impradice, J. P. A. Fairclough, N. J. Terrill and A. J. Ryan, *Macromolecules*, 2010, **43**, 2389-2405.
11 K. Cui, L. Meng, N. Tian, W. Zhou, Y. Liu, Z. Wang, J. He and L. Li, *Macromolecules*, 2012, **45**, 5477-5486.
12 Y. F. Huang, J. Z. Xu, J. S. Li, B. X. He, L. Xu and Z. M. Li, *Biomaterials*, 2014, **35**, 6687-6697.
13 Y. F. Huang, J. Z. Xu, J. Y. Xu, Z. C. Zhang, B. S. Hsiao, L. Xu and Z. M. Li, *J. Mater. Chem. B*, 2014, **2**, 971-980.
14 L. Xu, Y. F. Huang, J. Z. Xu, J. Xu and Z. M. Li, *RSC Adv.*, 2014, **4**, 1512-1520.
15 Y. H. Chen, Z. Y. Huang, Z. M. Li, J. H. Tang and B. S. Hsiao, *RSC Adv.*, 2014, **4**, 14766-14776.
16 L. Xu, C. Chen, G. J. Zhong, J. Lei, J. Z. Xu, B. S. Hsiao and Z. M. Li, *ACS Appl. Mater. Interfaces*, 2012, **4**, 1521-1529.
17 Y. Pan, S. Shi, W. Xu, G. Zheng, K. Dai, C. Liu, J. Chen and C. Shen, *J. Mater. Sci.*, 2014, **49**, 1041-1048.
18 J. Yang, K. Wang, H. Deng, F. Chen and Q. Fu, *Polymer*, 2010, **51**, 774-782.
19 K. Wang, F. Chen, Q. Zhang and Q. Fu, *Polymer*, 2008, **49**, 4745-4755.
20 S. Fellahi, B. Favis and B. Fisa, *Polymer*, 1996, **37**, 2615-2626.
21 Z. Guo, B. Hagström, *Polym. Eng. Sci.*, 2013, **53**, 2035-2044.
22 R. R. Hegde, J. E. Spruiell, G. S. Bhat, *Polym. Int.*, 2014, **63**, 1112-1121.
23 K. Wang, S. Liang, J. Deng, H. Yang, Q. Zhang, Q. Fu, D. Xia, D. Wang and C. C. Han, *Polymer*, 2006, **47**, 7131-7144.
24 C. Zhao, H. Qin, F. Gong, M. Feng, S. Zhang and M. Yang, *Polym. Degrad. Stab.*, 2005, **87**, 183-189.
25 Q. Yuan, Y. Yang, J. Chen, V. Ramuni, R. Misra and K. Bertrand, *Mater. Sci. Eng. A*, 2010, **527**, 6699-6713.

26 M. Tanniru and R. Misra, *Mater. Sci. Eng. A*, 2005, **405**, 178-193.
27 K. Wang, N. Li, K. Ren, Q. Zhang, Q. Fu, *Composites Part A*, 2014, **61**, 84-90.
28 J. Yang, C. Wang, K. Wang, Q. Zhang, F. Chen, R. Du and Q. Fu, *Macromolecules*, 2009, **42**, 7016-7023.
29 S. Liang, K. Wang, H. Yang, Q. Zhang, R. Du, Q. Fu, *Polymer*, 2006, **47**, 7115-7122.
30 H. H. Li, J. C. Liu, D. J. Wang and S. K. Yan, *Colloid. Polym. Sci.*, 2003, **281**, 973-979.
31 U. Stachewicz, F. Modaresifar, R. J. Bailey, T. Peijs and A. H. Barber, *ACS Appl. Mater. Interfaces*, 2012, **4**, 2577-2582.
32 S. Jiang, G. Duan, J. Schöbel, S. Agarwal and A. Greiner, *Compos. Sci. Technol.*, 2013, **88**, 57-61.
33 J. Chen, W. Yang, G. Yu, M. Wang, H. Ni and K. Shen, *J. Mater. Process. Technol.*, 2008, **202**, 165-169.
34 H. Zheng, B. Wang, G. Zheng, Z. Wang, K. Dai, C. Liu and C. Shen, *Ind. Eng. Chem. Res.*, 2014, **53**, 6211-6220.
35 P. de Gennes, *J. Chem. Phys.*, 1974, **60**, 5030-5042.
36 I. Dukovski and M. Muthukumar, *J. Chem. Phys.*, 2003, **118**, 6648-6655.
37 M. Sabino, G. Ronca and A. Müller, *J. Mater. Sci.*, 2000, **35**, 5071-5084.
38 H. Han, X. Wang and D. Wu, *J. Chem. Technol. Biotechnol.*, 2013, **88**, 1200-1211.
39 S. Liang, H. Yang, K. Wang, Q. Zhang, R. Du and Q. Fu, *Acta Mater.*, 2008, **56**, 50-59.
40 J. T. Yeh, S. C. Lin, C. W. Tu, K. H. Hsie and F. C. Chang, *J. Mater. Sci.*, 2008, **43**, 4892-4900.
41 A. Turner-Jones and A. Cobbold, *J. Polym. Sci. B Polym. Lett.*, 1968, **6**, 539-546.
42 K. Wang, K. Mai, Z. Han and H. Zeng, *J. Appl. Polym. Sci.*, 2001, **81**, 78-84.
43 G. Strobl and M. Schneider, *J. Polym. Sci. Polym. Phys. Ed.*, 1980, **18**, 1343-1359.
44 H. Bai, F. Luo, T. Zhou, H. Deng, K. Wang and Q. Fu, *Polymer*, 2011, **52**, 2351-2360.
45 R. R. Hegde, J. E. Spruiell and G. S. Bhat, *Polym. Int.*, 2014, **63**, 1112-1121.
46 F. Mai, D. Pan, X. Gao, M. Yao, H. Deng, K. Wang, F. Chen and Q. Fu, *Polym. Int.*, 2011, **60**, 1646-1654.
47 M. Camargo, F. M. M. Camargo and C. R. Wolf, *Int. J. Polym. Anal. Charact.*, 2008, **13**, 49-65.
48 S. Ratner, A. Weinberg and G. Marom, *Polym. Compos.*, 2003, **24**, 422-427.
49 H. Goossens, S. Jain, M. van Duin and P. Lemstra, *Polymer*, 2005, **46**, 8805-8818.
50 F. Mai, K. Wang, M. Yao, H. Deng, F. Chen and Q. Fu, *J. Phys. Chem. B*, 2010, **114**, 10693-10702.
51 B. Pukánszky, I. Mudra and P. Staniek, *J. Vinyl. Addit. Technol.*, 1997, **3**, 53-57.
52 Y. Gao, K. Ren, N. Ning, Q. Fu, K. Wang and Q. Zhang, *Polymer*, 2012, **53**, 2792-2801.

Figure Captions

Figure 1. (a) Schematic of the shear-induced crystallization setup used in this study; (b) digital photo of the shear-induced USKM; (c) SEM image of the shear-induced USKM with low magnification. The numbers in (a) represents: 1-ferrum frame; 2-UHMWPE/xylene solution; 3-stir bar; 4-motor. The blue arrow in (b) refers to the shear direction.

Figure 2. DSC melting curves of the as-received LLDPE, HDPE granules and shear-induced USKM (samples with 5-8 mg were respectively heated to 180 ^{o}C from room temperature at a heating rate of 10 ^{o}C/min).

Figure 3. SEM images of the shear-induced USKM. The blue arrow refers to the shear direction.

Figure 4. AFM image of the shear-induced USKM. The shear direction is horizontal.

Figure 5. (a) DSC curves of isothermal crystallization for USKM/LLDPE composite and pure LLDPE; (b) normalized relative crystallinity (X_t) as a function of crystallization time.

Figure 6. 2D-WAXD (a_1, a_2) and 2D-SAXS (b_1, b_2) patterns of samples: pure LLDPE (a_1, b_1), USKA/LLDPE composite (a_2, b_2). The shear direction is horizontal.

Figure 7. (a) Azimuthal distribution integrated from $(200)_m$ crystal plane of USKM/LLDPE composite; (b) 1D-WAXD curves of pure LLDPE and USKM/LLDPE composite.

Figure 8. (a) Calculation method of long period (L), lamellar thickness (L_c) obtained from the one-dimensional correlation function $K(z)$; (b) curves of the one-dimensional electron density correlation function of the pure LLDPE and USKM/LLDPE composite.

Figure 9. SEM images of etched surface of USKM/LLDPE composite. The white arrow refers to flow direction of USKM.

Figure 10. (a) DSC melting curves of pure LLDPE and USKM/LLDPE composite; (b) amplified image of the area in the dashed square of (a).

Figure 11. Representative stress-strain curves of pure LLDPE and USKM/LLDPE composites.

Tables

Table 1. The crystalline data obtained from the 2D-WAXD and 2D-SAXS results.

Samples	X_c (%)	L_c (nm)	L (nm)
LLDPE	36.44	5.68	12.78
USKM/LLDPE	39.13	5.80	13.02

Table 2. Mechanical parameters obtained from stress-strain curves.

Samples	E (MPa)	σ_y (MPa)	σ (MPa)	ε (%)
LLDPE	80.6 ± 5.3	5.5 ± 0.7	13.2 ± 0.6	1468.0 ± 32
USKM/LLDPE	112.5 ± 4.6	10.5 ± 1.2	16.1 ± 0.8	1084.2 ± 45